European Journal of Medicinal Chemistry 166 (2019) 243–255

Contents lists available at ScienceDirect

European Journal of Medicinal Chemistry

journal homepage: http://www.elsevier.com/locate/ejmech

Research paper

Synthesis of new derivatives of boehmeriasin A and their biological evaluation in liver cancer

Ece Akhan Güzelcan [a], Ian R. Baxendale [b, *], Rengul Cetin-Atalay [a, **], Marcus Baumann [c, ***]

[a] Graduate School of Informatics, Cancer Systems Biology Laboratory, METU, 06800, Ankara, Turkey
[b] Department of Chemistry, University of Durham, South Road, DH1 3LE, Durham, UK
[c] School of Chemistry, University College Dublin, Science Centre South, Belfield, Dublin 4, Ireland

ARTICLE INFO

Article history:
Received 9 September 2018
Received in revised form
2 January 2019
Accepted 23 January 2019
Available online 24 January 2019

Keywords:
Boehmeriasin A
Natural product analogs
Liver cancer
Cell cycle analysis

ABSTRACT

Two series of boehmeriasin A analogs have been synthesized in short and high yielding processes providing derivatives differing either in the alkaloid's pentacyclic scaffold or its peripheral substitution pattern. These series have enabled, for the first time, comparative studies into key biological properties revealing a new lead compound with exceptionally high activity against liver cancer cell lines in the picomolar range for both well (Huh7, Hep3B and HepG2) and poorly (Mahlavu, FOCUS and SNU475) differentiated cells. The cell death was characterized as apoptosis by cytochrome-C release, PARP protein cleavage and SubG1 cell cycle arrest. Subsequent testing associated apoptosis via oxidative stress with *in situ* formation of reactive oxygen species (ROS) and altered phospho-protein levels. Compound **19** decreased Akt protein phosphorylation which is crucially involved in liver cancer tumorigenesis. Given its simple synthetic accessibility and intriguing biological properties this new lead compound could address unmet challenges within liver cancer therapy.

1. Introduction

Primary liver cancer (hepatocellular carcinoma, HCC), is the sixth most frequent cancer type and the second highest cause of cancer-related death worldwide [1]. Viral infections with hepatitis B or C, alcoholic injury, obesity and other factors inducing cirrhosis and chronic liver disease are additional major risk contributors for HCC [2–4]. It is also expected that the rate of liver cancer and associated deaths will increase in the coming years due to the global epidemic of non-alcoholic fatty liver disease (NAFLD) [5]. Despite these well-known etiological factors, liver cancer remains one of the most lethal types of cancer, due to the very limited therapeutic options that offer significant clinical benefits [6]. Liver resection, transplantation and chemoembolization are still the most relied upon options, however, not all the patients can meet the criteria for these treatments [7]. Meanwhile, patients with advanced HCC suffer from the lack of effective therapy. The first FDA approved drug Sorafenib (**5**, Fig. 1), which is a multi-kinase inhibitor, can only improve patients' median survival for about 3 months [8]. Very recently, the closely related multi-kinase inhibitor Regorafenib was used in patients as a second line treatment. The mean survival period was 10 months compared to a placebo (~8 months) [9].

To address these challenges in the arena of liver cancer [10], we decided to investigate the chemical synthesis and biological evaluation of new analogs of the known plant alkaloid boehmeriasin A.

Boehmeriasin A (**1**, Fig. 1) is a pentacyclic phenanthroquinolizidine alkaloid recently isolated from the ethanolic extract of *boehmeria siamensis* Craib [11], a plant that has long been used in south-east Asia for the treatment of rheumatism as well as skin diseases such as urticaria (hives). Through extensive biological studies, it has been revealed that **1** possesses significant activity against several cancer cell lines commonly exceeding the potency of Taxol by at least tenfold. The nanomolar cytotoxic activity of boehmeriasin A was established for various cancer cells, originating from lung, colon, breast, prostate, kidney cancers, and leukemia [12]. In addition to this anti-cancer activity boehmeriasin A also causes G1 cell cycle arrest, cellular differentiation, affects cellular

* Corresponding author.
** Corresponding author.
*** Corresponding author.
E-mail addresses: i.r.baxendale@durham.ac.uk (I.R. Baxendale), rengul@metu.edu.tr (R. Cetin-Atalay), marcus.baumann@ucd.ie (M. Baumann).

https://doi.org/10.1016/j.ejmech.2019.01.056
0223-5234/

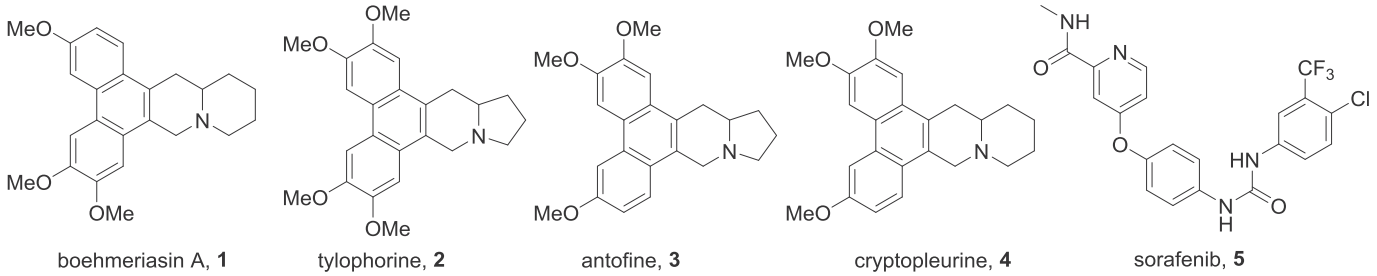

Fig. 1. Structures of racemic boehmeriasin A **1**, related alkaloids (**2**–**4**) and sorafenib.

morphology and results in lipid droplet accumulation in breast cancer cells [13]. It was furthermore found that boehmeriasin A shares this promising anti-cancer activity with other members of the phenanthroquinolizidine and -pyrrolizidine alkaloids such as tylophorine (**2**), antofine (**3**) and cryptopleurine (**4**) (Fig. 1) [14–21]. Topoisomerases and SIRT2 were proposed as potential biological targets of Boehmeriasin A [24].

Driven by the promising bioactivity reports, many successful total syntheses of these intriguing cytotoxic alkaloids have been disclosed [12,22–24]. Despite these efforts neither the molecular target nor the mode of action of these important structures have been identified and detailed SAR studies are lacking, which severely hamper development of further boehmeriasin A based leads. To establish this missing key data, we wished to evaluate boehmeriasin A as well as several new analogs in the context of human epithelial cancers especially in liver cancer.

1.1. Analog synthesis

Upon analysis of the parent pentacyclic scaffold of boehmeriasin A (**1**) and its closely related natural products (**2**–**4**) we decided to design and synthesize two series of target compounds to study their structure-activity relationship. The first series would retain the oxygenation pattern of boehmeriasin A but introduce alterations in the connectivity of the fused ring system, whereas the second series would conserve the original pentacyclic framework while modifications to the embedded quinolizidine system would be made.

To create these two series, we decided to exploit a synthetic route to boehmeriasin A itself which we had previously developed (Scheme 1) [24]. The route is based on an efficient 7-step sequence in which a Perkin reaction is followed by an esterification to yield building block **8** that was then converted into the phenanthrene unit **9** by a $FeCl_3$-mediated oxidation. The pendant ester functionality was then reduced to an alcohol and activated as the corresponding chloride (**10**) to allow coupling with pipecholic acid (**11**). Treatment of **12** with polyphosphoric acid (PPA) leads to ring closure *via* a Friedel-Crafts acylation reaction and furnishes ketone **13** that upon full reduction gives the desired natural product **1**. This approach was deemed very attractive as it had been shown to be robust and scalable and furthermore allows the introduction of the desirable variations on different moieties of the parent structure of **1**.

The synthesis of the first analog series utilized intermediates **8** and **9** that were independently elaborated by amide coupling with aminopropyl imidazole (**14**, Scheme 2). The aminopropyl imidazole was selected as a hydrophylic appendage to mimic the quinolizidine substructure of **1** and to improve bioavailability. Furthermore, it was intended to modulate the planarity of the phenanthrene system by omitting the central C-C bond in some of the analogs, which would enable us to evaluate the likelihood of these entities acting via DNA interchelation.

Compounds **8** and **9** were hydrolyzed under basic conditions rendering the corresponding carboxylic acid derivatives that were subsequently activated by CDI and coupled with aminopropyl imidazole (**14**) to furnish the desired amides **15** and **16** in good yield. In addition, both amides were treated with LAH (2.5 equiv.) to obtain the corresponding amines **17** and **18** allowing to establish the effect of having an amide versus an amine incorporated into these structures, which could have implications due to altered H-bonding patterns.

With the first analog series in hand we turned our attention to a second series in which we envisaged studying alterations on the

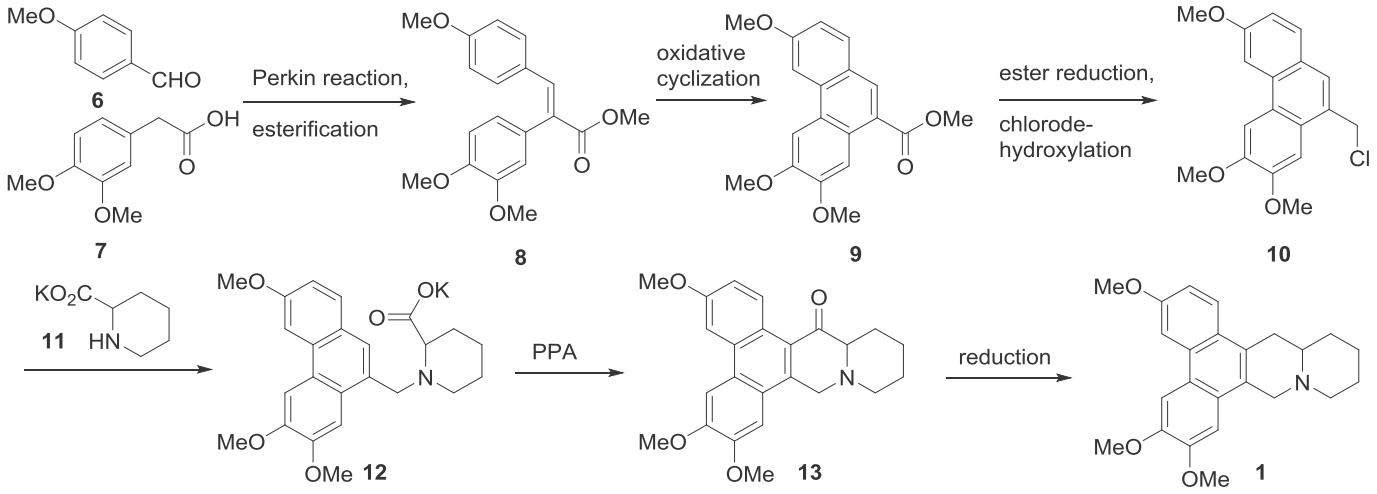

Scheme 1. Previous synthesis of racemic boehmeriasin A (**1**).

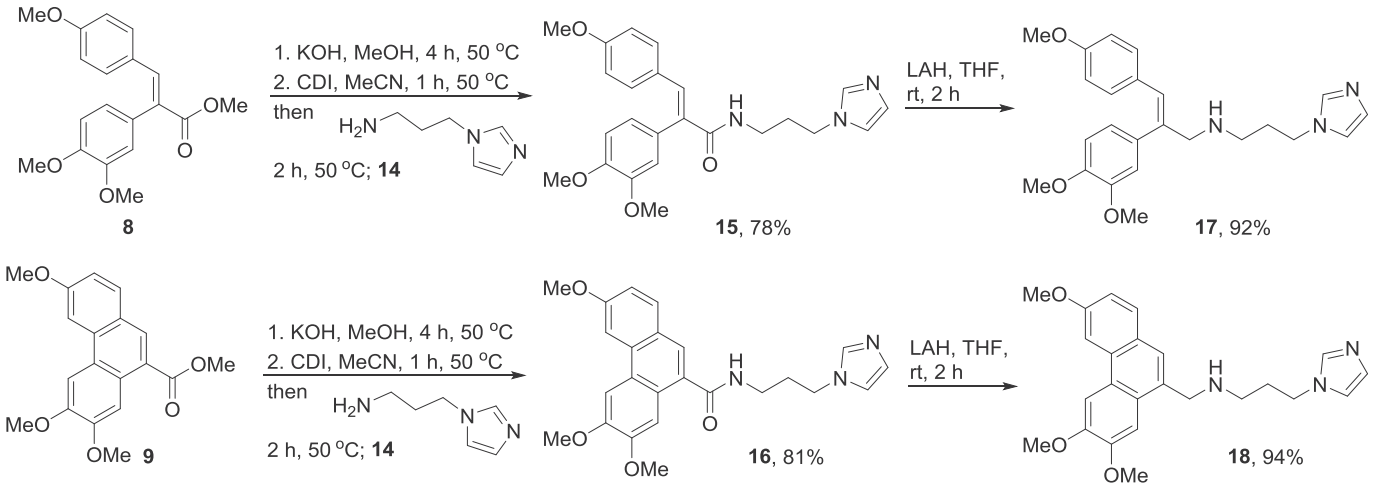

Scheme 2. Synthesis of analogs **15**–**18** (Series 1).

pentacyclic framework of boehmerisain A. Specifically, we decided to explore manipulations of the carbonyl of **13** by means of its reduction to the corresponding alcohol derivatives. The synthesis of the desired alcohols was readily accomplished by reduction of **13** by LAH (2.0 equiv.) giving a diastereomeric mixture of alcohol products **19a** and **19b** in a 1:2 ratio. Pleasingly, it was possible to separate this mixture by preparative TLC to undertake characterization and subsequent biological evaluation of the individual diastereomers. Additionally, single crystal X-ray diffraction experiments were used to identify the major diastereomer **19b** as the *trans*-alcohol product (Scheme 3).

Together with boehmeriasin A (**1**) and its carbonyl derivative **13**, these individual alcohol derivatives **19a** and **19b** therefore represent the second series of analogs available for detailed biological testing (Fig. 2).

2. Biological studies

2.1. Biological activities of first series of boehmeriasin A analogs

Commencing our studies with boehmeriasin A analogs **15**–**18** we analyzed their cellular toxicity against different hepatocellular carcinoma cells, namely Huh7 and Mahlavu. As pointed out earlier we wished to establish whether simplified structures possessing a conformationally open ring system would still impart significant cytotoxicity, whilst improving solubility by introduction of an imidazole appendage. However, to our surprise it was found that these analogs displayed either very moderate activity (compounds **16** and **17** IC_{50} 10–54 μM) or no activity (compounds **15** and **18,** Table 1). Additionally, the presence of an amide or amine linkage as well as the central biaryl bond appears to be irrelevant with regards to activity against these cell lines. Whilst somewhat unexpected this finding establishes clearly that the pentacyclic framework of the boehmeriasins is crucial for their sub-micromolar biological activity which had not been demonstrated before. This furthermore highlights the importance of the embedded quinolizidine substructure and prompted us to evaluate analogs of our second series next.

2.2. Cytotoxicity of second series of boehmeriasin A derivatives

To verify the anticipated biological activity of the parent boehmeriasin A (**1**) and its analogs (**12**, **13**, **19**) an initial screen against different epithelial cancer cells, namely liver (Huh7), breast (MCF7) and colon (HCT116) carcinoma cells was performed. The cytotoxicity of each compound was assessed by sulforhodamine B (SRB) assay. IC_{50} values of the synthesized compounds were calculated for each cell line following treatment for 72 h (Table 2). The high cytotoxicity found in all cancer cell types may address the possible role of these compounds on common cancer activated pathways.

In general, boehmeriasin A (**1**) and its hydroxy analog **19** (as 1:2 mixture of diastereomers) were identified as promising anti-cancer compounds due to their low nanomolar IC_{50} values. Although ketone derivative **13** showed moderate cytotoxicity, when compared to **1** and **19** its bioactivity was low despite the only minor alteration of its structure. Additionally, the carboxylate species **12** had no cytotoxic bioactivity against these cancer cells, possibly because it does not easily permeate into cells due to its ionic nature. Furthermore, this result is in line with the loss of activity seen for the other 'open-structured' analogs **15**–**18**.

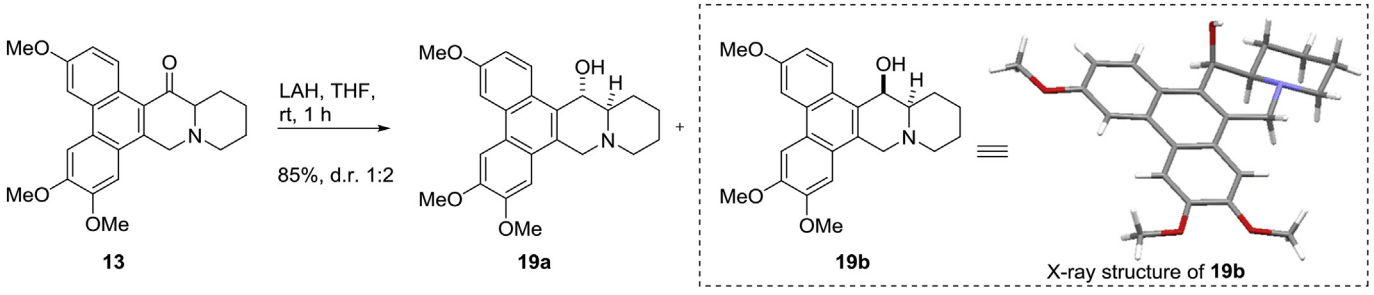

Scheme 3. Synthesis of analogs **19a** and **19b** from ketone **13** (Series 2).

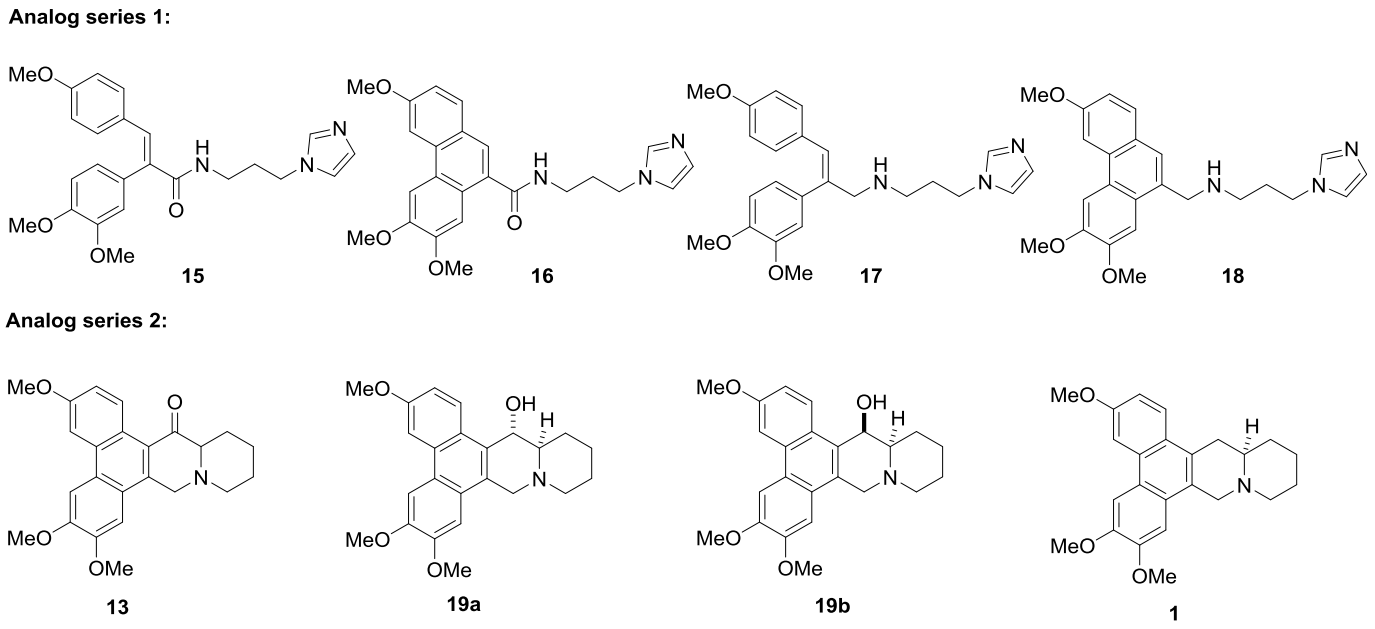

Fig. 2. Overview of both series of new boehmeriasin A analogs.

Table 1
Cytotoxicity of compounds **15**–**18** evaluated in HCC cells.

IC_{50} Values (μM)		
Compound	Huh7	Mahlavu
15	NI	NI
16	19.2	54
17	9.3	13.8
18	NI	NI

*NI: No inhibition.

Table 2
Initial screening of compounds **1**, **12**, **13** and **19**.

IC_{50} Values (μM)			
Compound	Huh7	MCF7	HCT116
1	0.008	0.005	0.7
19	0.002	0.001	<0.001
12	NI	NI	NI
13	12	7	8.1

*NI: No inhibition.

Considering the specific lack of any HCC targeted chemotherapeutic agents and based upon our specific aim in this study, we furthermore tested these compounds (**1**, **12**, **13** and **19**) against various liver cancer cell lines and normal transformed breast epithelial cells since there are no transformed normal liver hepatocytes available. Therefore, we assessed the IC_{50} values of these compounds in a HCC cell panel (Huh7, Mahlavu, SNU475, FOCUS, Hep3B and HepG2) (Table 3).

Similar to our results presented in Table 2, compounds **1** and **19** were found to be significantly cytotoxic in all cell types of HCCs. Crucially, **1** and **19** displayed nanomolar IC_{50} values not only for well differentiated HCC cells such as Huh7, Hep3B and HepG2 but also for poorly differentiated and more aggressive cells as tested here, namely, Mahlavu, FOCUS and SNU475. Furthermore, normal transformed epithelial cells were less sensitive to compounds **1** and **19**. Our data showed significant cytotoxic effects of compounds in the nanomolar range in cancer cells while the cytotoxic effect on normal transformed cells was diminished (Table 3). The higher IC_{50} found in normal like HepG2 cells further supported the cancer-specific activity of these compounds. Therefore, **1** and **19** can be considered potential anti-cancer drug candidates in liver cancer cells. On the other hand, **13** displayed limited cytotoxic activity and **12** had no activity in any type of HCC cells (data not shown).

*2.3. Real-time assessment of hepatocellular carcinoma cell growth upon treatment with compounds **1** and **19***

A real-time cell electronic sensing (xCELLigence RTCA analysis) assay was used to evaluate the bioactivities of Boehmeriasin A and its analog **19** on well differentiated Huh7 cells and poorly differentiated aggressive mesenchymal Mahlavu cells (25). According to the data obtained from this analysis, the time dependent IC_{50} values were calculated (Table 4). Compounds **1** and **19** caused significant growth inhibition in both cells. Drug resistant Mahlavu

Table 3
Cytotoxicity of compounds in HCC cell panel.

Compound	IC_{50} Values (μM)							
	Huh7	Hep3B	HepG2	Mahlavu	SNU475	FOCUS	MCF12A	MCF10A
1	0.008	0.016	0.06	0.016	0.014	0.02	0.07	0.14
19	0.002	0.017	2.7 ± 0.9	0.01	0.015	0.012	2<	0.2
12	NI	NI	NI	NI	NI	NI	NI	NT
13	12	45	NI	35	19.1	5	NI	NT

*NI: No inhibition, NT: Not tested.

Table 4
Time dependent IC_{50} values of compounds **1** and **19**.

IC_{50} Values (μM)						
Compound	Huh7			Mahlavu		
	24 h	48 h	72 h	24 h	48 h	72 h
1	1.4 μM	0.7 μM	0.7 μM	0.2 μM	0.4 μM	0.6 μM
19	0.8 μM	0.5 μM	0.4 μM	0.01 μM	0.004 μM	0.01 μM

cells were prominently more sensitive to **19** (Fig. 3). The real-time growth inhibition pattern suggested a cell cycle arrest in cells treated with **1** and **19**, as DMSO treated cells retain their proliferation profile until they become confluent.

The curvature of the real time cell death data and the measured IC_{50} values imply that the cell death associated with these compounds could be apoptosis. The differences of IC_{50} values between SRB end point colorimetric assay and the real time cell growth assays can be due to the evaluation of distinct cellular elements. While SRB detects the total protein levels, RTCA is dependent on the cell surface attachment properties of each different cell. During apoptosis there is a high destruction of cellular proteins which leads to less colorimetric data collection. Therefore, it is common to observe IC_{50} differences between cell death detection techniques. Hence in this study, we established the bioactivities of the new boehmeriasin A analogs using two complementary techniques.

2.4. Characterization of cell death mechanism induced by boehmeriasin derivatives

The cell death mechanism of the cells treated with boehmeriasin A or its derivatives was initially analyzed by observing the release of cytochrome-C which was examined via fluorescence microscopy (Fig. 4A). Camptothecin (CPT) was used as positive control for cytochrome-C release, showing that cytochrome-C levels in cells treated with **1** and **19** were comparable to the positive control. A significant increase in the release of cytochrome-C in cells treated with **1** and **19** indicates apoptotic cell death.

The activation of apoptotic pathways by boehmeriasin A derivatives was further studied by evaluating the status of one of the most well-known apoptotic proteins, PARP. Here a significant increase in PARP cleavage in the cells treated with **19** was identified and became significant within 72 h in cells. Compared to boehmeriasin A itself, the hydroxy-derivative **19** displayed a more significant effect on PARP cleavage that is paralleled by its increased cytotoxic effect on liver cancer cells (Fig. 4B).

During cellular apoptosis, many biochemical changes occur. Once the apoptosis mechanism is triggered DNA fragmentation, phosphatidylserine flipping to the outer surface of the cells and some morphological changes such as smaller cell size, chromatin condensation and formation of apoptotic bodies eventually occur. Hoechst is a fluorescence dye that attaches to DNA of both dead and living cells and makes their nucleus visible. The intensity of Hoechst staining (chromatin condensation), structure of nucleus and formation of apoptotic bodies are the initial indicators of cellular apoptosis. The Hoechst staining of **1** and **19** treated cells

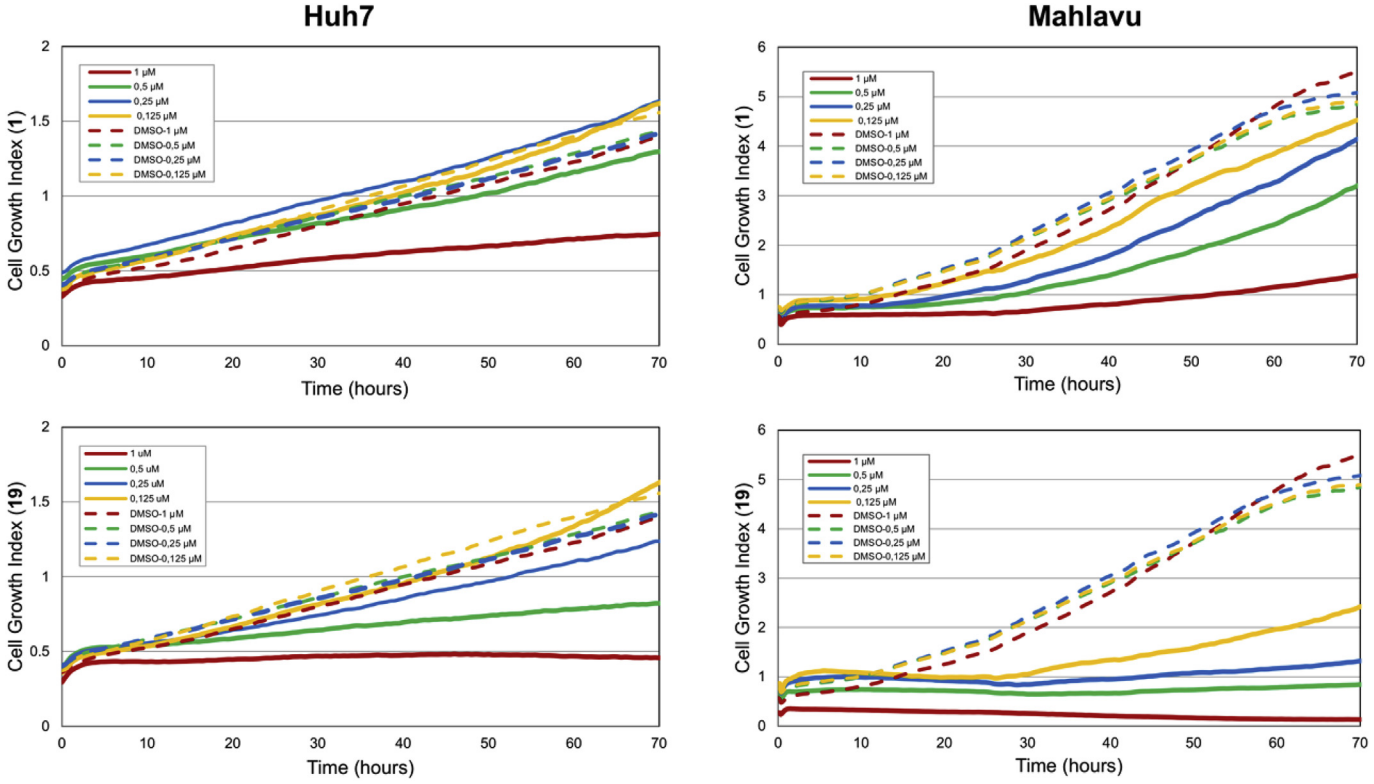

Fig. 3. xCELLigence RTCA analysis. Cell growth index with various concentrations of the compounds **1**, **19** and their corresponding DMSO solvent controls on Huh7 and Mahlavu cell lines.

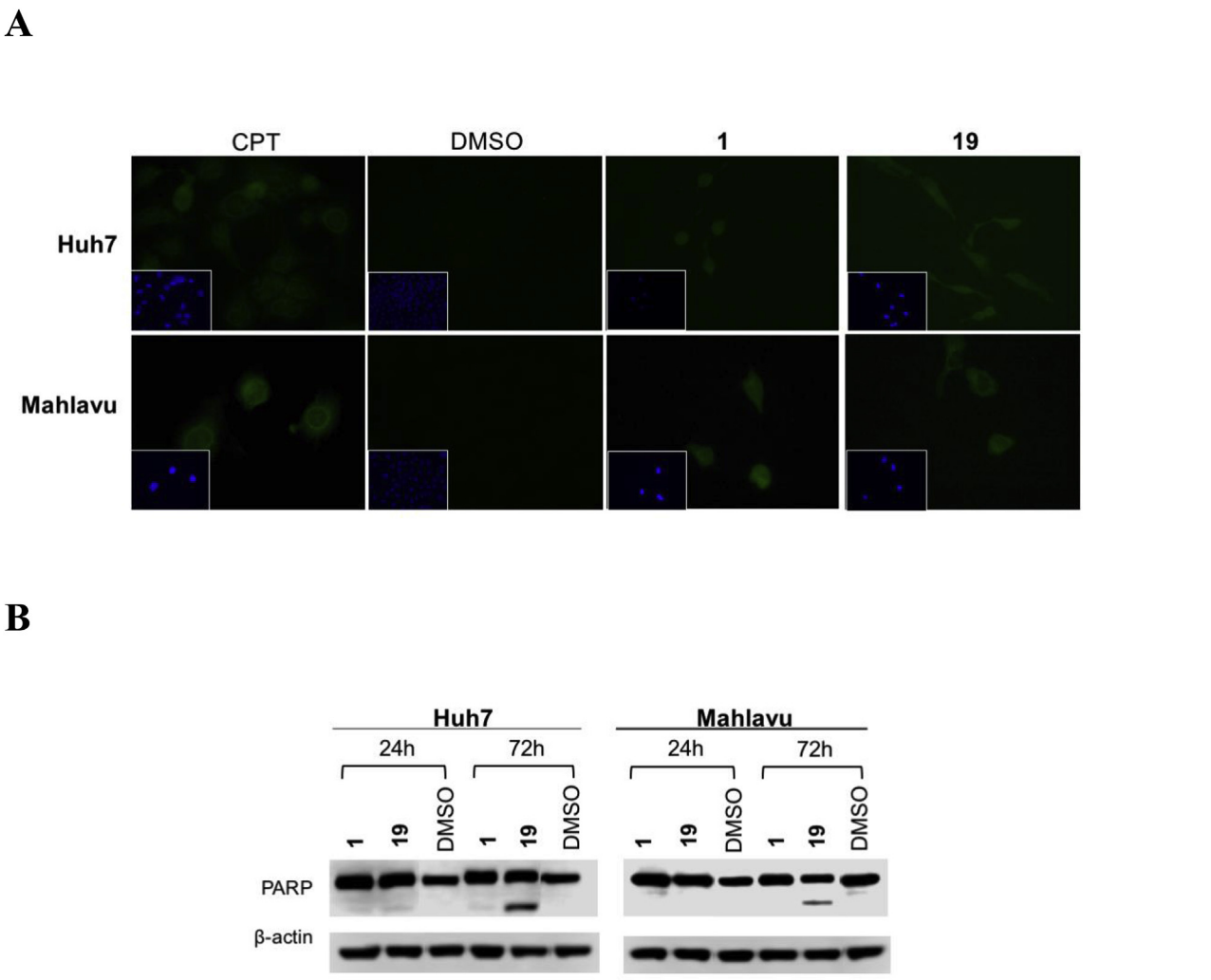

Fig. 4. Analysis of apoptotic processes in cells treated with Boehmeriasin A derivatives. (A) The evaluation of Cytochrome C (green) release in Huh7 and Mahlavu cells treated with 1 μM **1** and **19**. The nuclei of cells were stained with Hoechst (blue). (B) PARP cleavage in Huh7 and Mahlavu cells treated with 1 μM **1** and **19** for 24 and 72 h. DMSO is used as solvent control. (C) The nucleus staining with Hoechst dye (blue) to identify the cellular apoptosis. White arrows indicate the apoptotic cells. (D) The Annexin V analysis of Huh7 and Mahlavu cells treated with 1 μM **1** and **19** for 24, 48 and 72 h. (For interpretation of the references to color in this figure legend, the reader is referred to the Web version of this article.)

showed many indicators of apoptosis (chromatin condensation and apoptotic body formation). The effect was increased at 72 h for all samples.

Moreover, the apoptosis of cells treated with **1** and **19** was further demonstrated with Annexin V assay via flow cytometry. Normally, phosphatidylserine (PS) residues are hidden in the membrane of living cells. Upon apoptosis, PS flips from the inner cell to the outer surface which then can be detected by Annexin V. This assay showed the sharp increase in apoptosis of cells treated with **1** and **19** for epithelial Huh7 cells at 72 h. The drug response was similar in Mahlavu cells at 72 h but **1** showed less dramatic effect on these cells. The Annexin V results thus supported the previous findings.

2.5. Cell cycle analysis of HCC cells treated with boehmeriasin derivatives

To identify the effect of the boehmeriasin derivatives on cell cycle progress, flow cytometry analysis was performed using propidium iodide (PI) staining in Huh7 and Mahlavu liver cancer cells. Upon treatment with compounds **1** and **19**, increasing levels of apoptotic cells along with SubG1 arrest were observed. The most significant increase was observed at 72 h. Derivative **19** resulted in the higher number of cells that accumulated at SubG1 phase. Additionally, HCC cells treated with **1** also led to an increase in SubG1, however, this effect became more notable after 72 h (Fig. 5 A, B). In addition, the effect of boehmeriasin A derivatives on the cell cycle was further investigated in Huh7 and Mahlavu cells by western blot analysis of the principal proteins which are involved in this process. Compounds **1** and **19** down-regulated Cyclin B1 (CDK1 regulator and mitotic initiator in the late G2 phase) and its companion CDK1 (essential for G1/S and G2/M phase transitions) levels in Huh7 cells. Treatment with **1** and **19** also reduced the CDK2 (G1 to S phase transition) and its regulator Cyclin E level, which became more significant at 72 h. Combined, these results indicate that boehmeriasin A derivatives induce cell cycle arrest at G2/M and SubG1 phases which is then followed by apoptosis of the cells (Fig. 5A).

The effect of these compounds on cell cycle protein expression is more pronounced on Huh7 cells (Fig. 5B). Mahlavu cells are

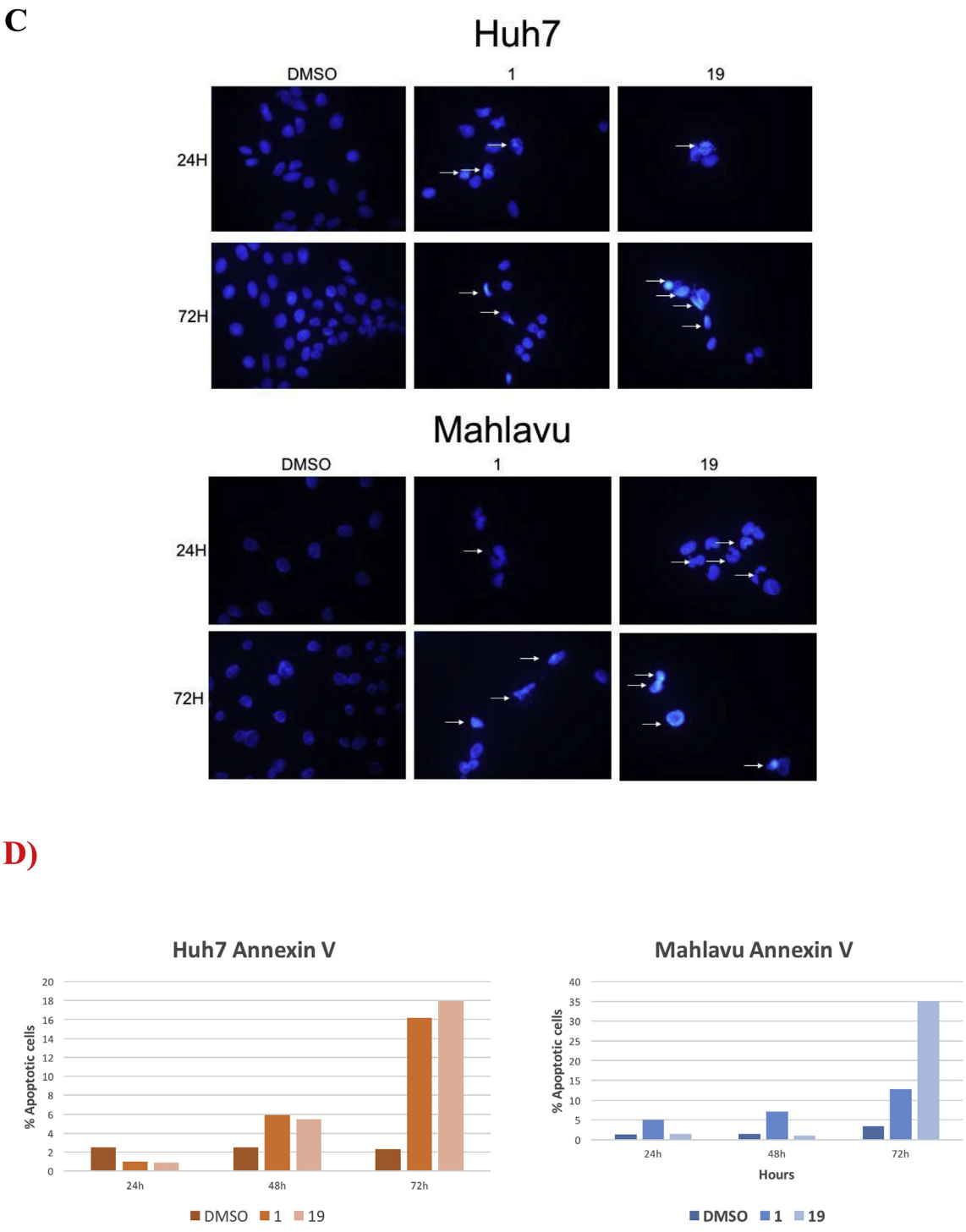

Fig. 4. (*continued*).

reported as more resistant to small molecule inhibitors due to PTEN deletion in PI3K/Akt signaling pathway [25]. However, the effect of compounds **1** and **19** can still be observed even in these cells. Furthermore, the active phosphorylated form of Akt protein is significantly down-regulated with compound **19** at 72 h (Fig. 5B).

2.6. Release of reactive oxygen species and stress mechanism induced by boehmeriasin derivatives

Reactive oxygen species (ROS), depending on their dose, can alter cellular pathways and promote cell cycle arrest and apoptosis in liver cancer cells [26]. The released ROS can be visualized using the 2,7-dichlorofluorescein diacetate (DCFH-DA) assay. The presence of fluorescence stain, which is detected via fluorescence microscopy, indicates ROS activity and thus cellular stress. Evaluating the presence of ROS in liver cancer cells that have been treated with boehmeriasin A and its derivatives showed that the ROS activity in cells incubated with **1** and **19** was significantly increased and became comparable to the positive control. The ROS activity increased with the time of incubation of **1** and **19** (Fig. 6A).

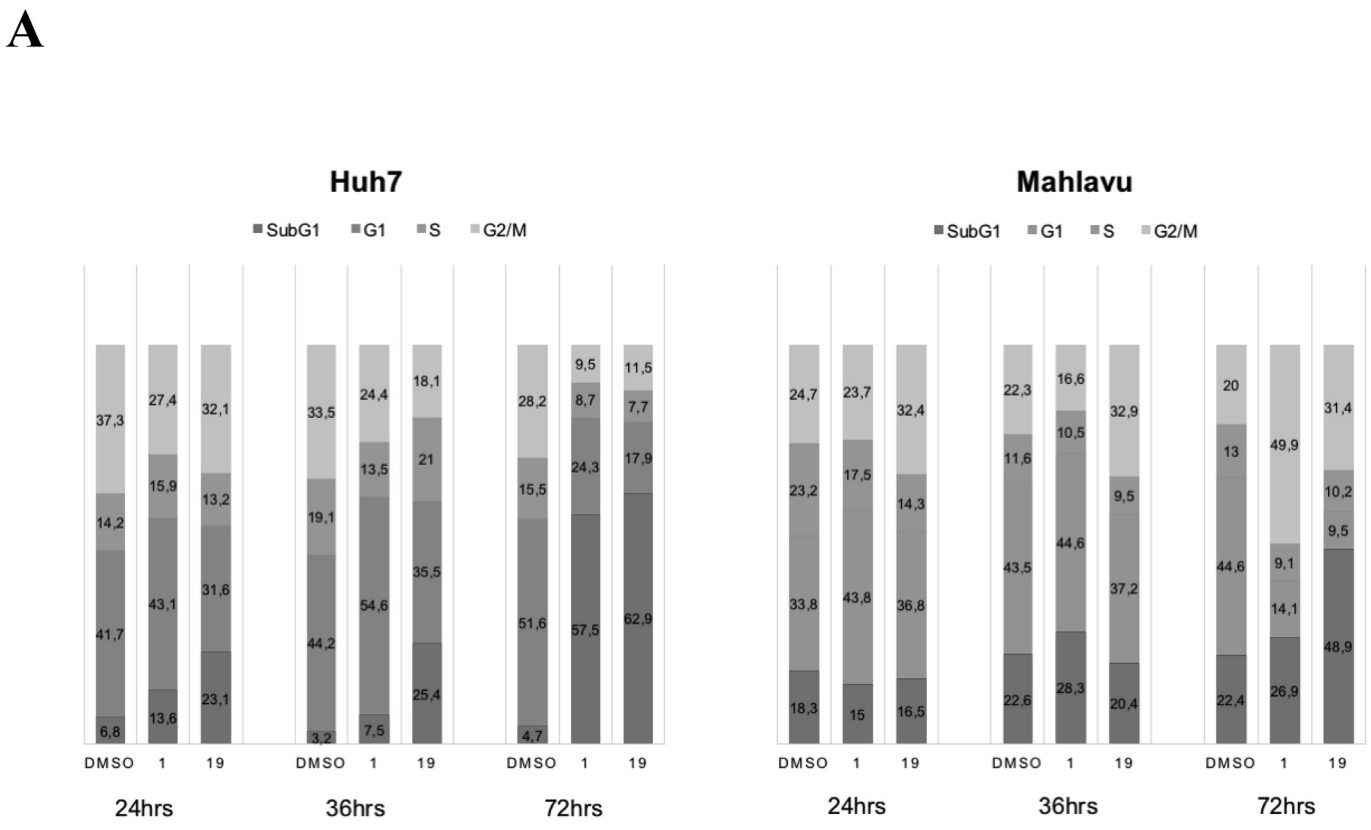

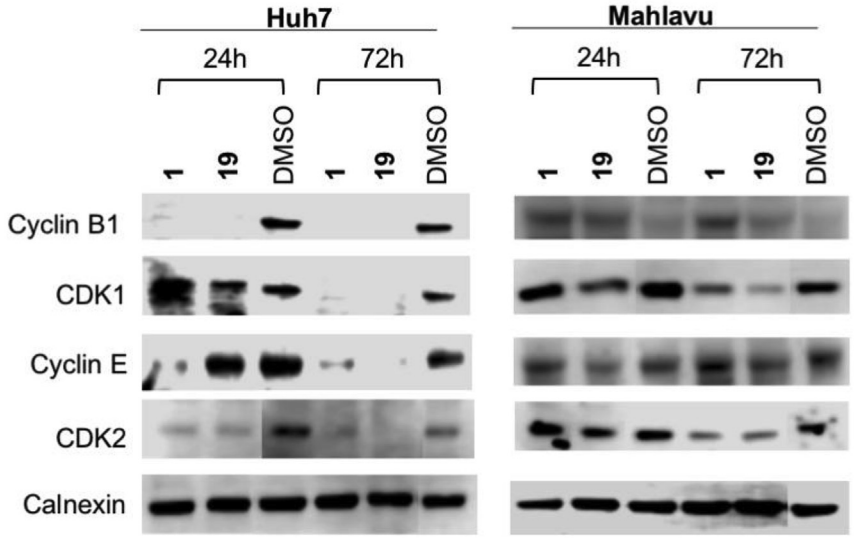

Fig. 5. The assessment of the cell cycle status of cells treated with boehmeriasin A derivatives. (A) The time dependent cell cycle analysis of treated Huh7 and Mahlavu cells with flow cytometry. (B) Comparative analysis of cell cycle protein expression in the presence of **1** and **19**. DMSO is used as the solvent control.

In addition, these Boehmeriasin derivatives induced oxidative stress, that was assessed by evaluating the phosphorylation status of the proteins involved in the ROS pathway via western blot [25]. It was found that Mahlavu and Huh7 cells treated with **1** and **19** led to a decrease of the phosphorylated Ser-966-ASK1 levels which is associated with cellular oxidative stress, though the effect on Mahlavu is being more prominent [25] (Fig. 6B). Mahlavu cells are characterized by a hyperactive PI3K/AKT pathway due to PTEN protein deletion and therefore we observe differential downstream P-SAPK/JNK protein levels. The stress protein SAPK/JNK phosphorylation was increased in Huh7 cells treated with both **1** and **19**. In Mahlavu cells the P-SAPK/JNK levels were differentially altered

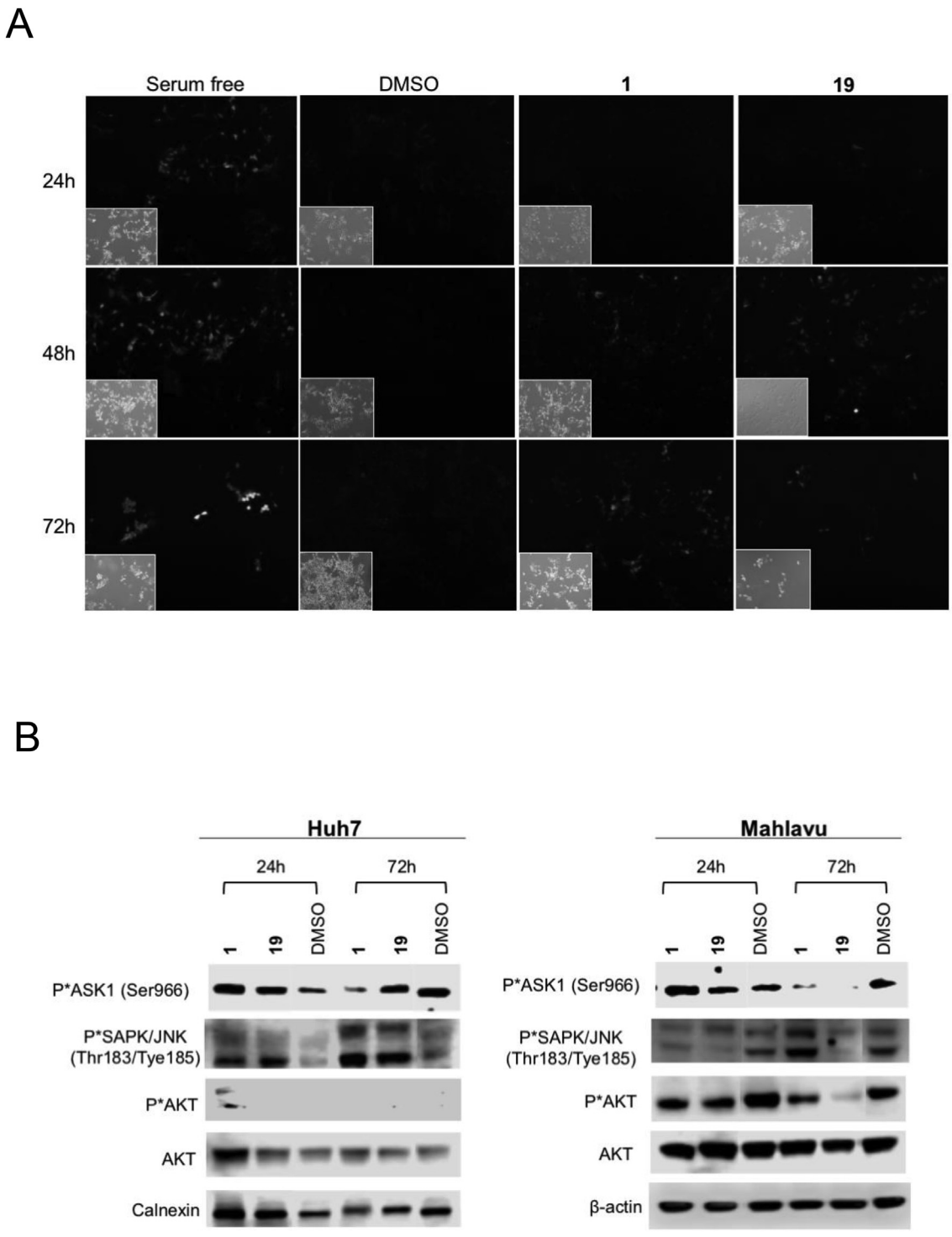

Fig. 6. The analysis of cellular stress mechanism. (A) The evaluation of ROS activity by DCHF-DA staining in Huh7 cells treated with boehmeriasin derivatives. DCFH-DA is a cell permeable dye, and, after uptake, it is cleaved by intracellular esterases to 2,7-dichlorodihydrofluorescin (DCFH2), which is trapped within the cells, and is oxidized to fluorescent 2,7-dichlorofluorescein (DCF) in the presence of ROS. The cells that grow in serum free medium were shown to induce ROS activity, therefore, we used serum free culture media as positive control. (B) The western blot analysis of the stress related proteins of boehmeriasin derivatives treated Huh7 and Mahlavu cells.

with **1** and **19** treatments in parallel to AKT phosphorylation status. The compound **19** decreases the p-AKT levels which is the active from of this protein required for cell survival. Our data indicates that the novel compound **19** gains its intriguing bioactivity through PI3K/AKT pathway modulation which is strategically involved in liver cancer tumorigenesis.

2.7. The bioactivity of individual hydroxy-analogs 19a and 19b on epithelial cancer and normal epithelial immortalized cells

Having determined that **19** (originally tested as a 1:2 mixture of diastereomers **19a** and **19b**) possessed the highest bioactivity, we decided to further study its individual diastereomers to establish

whether a preference of the relative stereochemistry manifests in differentiated activity. The separation of this mixture of diastereomers was accomplished by preparative thin layer chromatography yielding **19a** as the minor (lower R_f) and **19b** as the major (higher R_f) diastereomer in a 1:2 ratio. The individual hydroxy-analogs **19a** and **19b** were initially screened in human liver, colon and breast cancer cells along with immortalized transformed normal breast epithelial cells (Table 5). The data was verified with SRB results confirming not only that both hydroxy-analogs were highly active anti-cancer compounds but also **19b** displayed superior activity in the nanomolar range.

Correlating this intriguing finding with the single crystal X-ray structure secured for the major diastereomer **19b** (see Scheme 3) demonstrates that the highest activity results from the diastereomer having the hydroxy substituent *trans* to the methine proton and *syn* to the ring nitrogen. Although, the reason of this is not entirely clear at this point this finding might point to a specific binding mode of **19b** within its molecular target.

2.8. The induced apoptosis of individual hydroxy-analogs 19a and 19b

After we showed the cytotoxicity of **19a** and **19b** in nanomolar range, we further studied the cell death mechanism of these compounds in Huh7 and Mahlavu cells. Initially, treated cells were stained with Hoechst dye and their apoptotic morphologies were analyzed. The Hoechst staining of **19a** and **19b** treated cells showed a high number of apoptotic cells which possessed condensed chromatin and apoptotic bodies, compared to the DMSO control. The effect was increased for **19b** treated Huh7 cells which showed more apoptotic features compared to **19a** at 72 h. The apoptotic effect of compounds was similar in Mahlavu cells. A reduced number of remaining cells was observed after **19b** treatment in Mahlavu cells, therefore, the percentage of apoptotic cells had increased (Fig. 7A).

Table 5
Cytotoxicity of compounds **19a** and **19b** evaluated in different human cancer cells and normal transformed epithelial cells.

	Huh7	IC_{50} Values (μM)				
		Mahlavu	HCT116	MCF7	MCF10A	MCF12A
19a (minor)	0.306	0.05>	0.043	0.016	0.8	0.05>
19b (major)	0.017	0.05>	0.007	0.021	0.14	0.1

Furthermore, the Annexin V assay was utilized to analyze the apoptotic effect of **19a** and **19b** in more detail. Annexin V results showed the significant increase of apoptotic cells in **19b** treated cells, especially at 72 h. Similar to previous results, this assay further demonstrated the major compound **19b** had a severe effect on cellular apoptosis when compared to **19a** (Fig. 7B). Together these results supported the findings of SRB assay which revealed their high cytotoxicity.

In conclusion, we have successfully prepared two sets of new boehmeriasin A analogs featuring either a simplified structure or a complete pentacyclic framework as found in the parent alkaloid. Whilst the former was found to be significantly less active ($IC_{50} > 10$ μM) than boehmeriasin A, the latter series displayed superb anti-cancer activity across a range of cell lines. Minute structural changes from a ketone (**13**, H-bond acceptor) to a secondary alcohol (**19**, H-bond donor) have resulted in a 10,000-fold increase in activity, which is more pronounced in the *trans*-diastereomer (**19b**) and surpasses the activity of boehmeriasin A itself. Subsequent in-depth biological studies that were performed for the first time in HCC cells (well differentiated Huh7 and poorly differentiated aggressive Mahlavu cells) and have revealed a broad spectrum of activities including cell cycle arrest in the sub-G1 stadium, the generation of reactive oxygen species as well as the activation of apoptotic pathways through PARP cleavage. Moreover, Annexin V and Hoechst staining results further demonstrated the induction of apoptosis in drug treated cells. Due to the straightforward synthetic accessibility and the intriguing biological properties of our new lead compound **19b** we foresee its potential for future developments to address unmet challenges within liver cancer therapy.

3. Experimental section

3.1. Synthesis procedures for new compounds

Purity of all compounds was established via HPLC using an Agilent 1100 instrument with a Zorbax C18 column (4.6 × 100 mm) and UV-detection at 220 nm. An isocratic eluent system was used (60:40 MeCN:water, containing 0.1% TFA; 1 mL/min). All compounds displayed purities above 95% unless stated otherwise.

Rac-Boehmeriasin A, 1 and **3,6,7-trimethoxy-12,13,14,14a-tetrahydro-9*H*-dibenzo[f,h]-pyrido[1,2-b]isoquinolin-15(11*H*)-one, 13** were prepared as reported previously [24] and displayed purities of 97% and 96% respectively by HP-LC.

(*E*)-*N*-(3-(1*H*-Imidazol-1-yl)propyl)-2-(3,4-dimethoxyphenyl)-3-(4-methoxyphenyl)acryl-amide, 15: To a

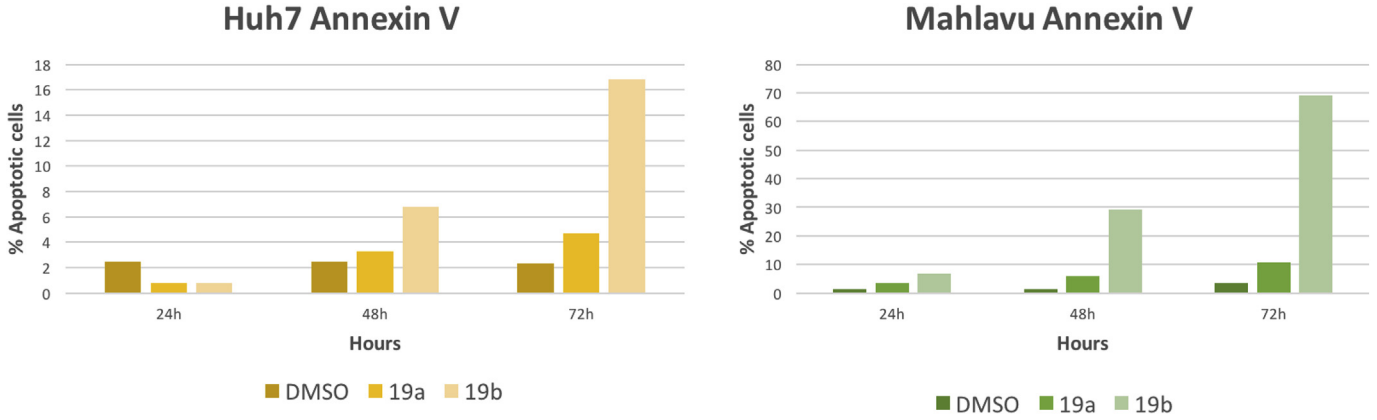

Fig. 7. The analysis of apoptosis. (A) The nucleus staining with Hoechst dye (blue) to identify the cellular apoptosis. White arrows indicate the apoptotic cells. (B) The Annexin V analysis of Huh7 and Mahlavu cells treated with 1 μM **19a** and **19b** for 24, 48 and 72 h. (For interpretation of the references to color in this figure legend, the reader is referred to the Web version of this article.)

solution of methyl (*E*)-2-(3,4-dimethoxyphenyl)-3-(4-methoxyphenyl)acrylate (**8**, 1.0 g, 3.05 mmol) in methanol (10 mL, 0.3 M) was added an aqueous solution of KOH (5.0 M, 5 mL, 8.3 equiv. KOH). The resulting mixture was stirred at 50 °C for 4 h when tlc analysis indicated full conversion of **8**. After neutralizing with aqueous HCl (1 M) and extraction (DCM/water, 2 × 50 mL) the organic layers were combined, dried over anhydrous sodium sulfate, filtered and evaporated to dryness under reduced pressure. The solid residue was dissolved in MeCN (15 mL) and combined with carbonyldiimidazole (CDI, 500 mg, 3.09 mmol, 1 equiv.). After heating this mixture for 1 h at 50 °C aminopropylimidazole (275 mg, 3.0 mmol, 1.0 equiv.) was added and the mixture was stirred at 50 °C for a further 2 h. After evaporation of the volatiles the crude product was extracted (DCM/water, 2 × 20 mL) and isolated as an off-white solid (1.0 g, 2.4 mmol, 78%) after drying over anhydrous sodium sulfate, filtration, evaporation and trituration from cold ethyl acetate.

^{1}H-NMR (400 MHz, $CDCl_3$): δ/ppm 7.68 (s, 1H), 7.34 (d, *J* = 1.2 Hz, 1H), 6.92 (d, *J* = 1.1 Hz, 1H), 6.91–6.87 (m, 3H), 6.83 (d, *J* = 1.3 Hz, 1H), 6.72 (dd, *J* = 8.2, 1.9 Hz, 1H), 6.64 (d, *J* = 1.9 Hz, 1H), 6.60 (d, *J* = 8.9 Hz, 2H), 5.73 (t, *J* = 6.1 Hz, 1H), 3.89 (t, *J* = 7.0 Hz, 2H), 3.86 (s, 3H), 3.72 (s, 3H), 3.66 (s, 3H), 3.23 (app q, *J* = 6.7 Hz, 2H), 1.90 (app p, *J* = 6.9 Hz, 2H). **^{13}C-NMR (100 MHz, $CDCl_3$):** δ/ppm 167.9 (C), 159.9 (C), 149.9 (C), 149.1 (C), 137.0 (CH), 136.8 (CH), 132.0 (2CH), 131.3 (C), 129.5 (CH), 128.5 (C), 127.4 (C), 122.0 (CH), 118.8 (CH), 113.7 (2CH), 112.6 (CH), 112.2 (CH), 56.0 (CH_3), 55.9 (CH_3), 55.1 (CH_3), 44.5 (CH_2), 37.2 (CH_2), 31.3 (CH_2). **IR (neat, ν/cm^{-1}):** 3375 (w), 2981 (s), 1655 (m), 1602 (m), 1509 (s), 1446 (m), 1252 (s), 1176 (m), 1139 (s), 1080 (m), 1019 (m), 959 (m), 833 (s), 738 (m), 620 (m). **HR-MS** (TOF-AP+) calculated for $C_{24}H_{28}N_3O_4$ 422.2080, found 422.2079. **HP-LC** (220 nm) Rt = 1.72 min (97% purity).

***N*-(3-(1*H*-Imidazol-1-yl)propyl)-3,6,7-trimethoxyphenanthrene-9-carboxamide, 16:** In analogy to the preparation of **15**, methyl 3,6,7-trimethoxyphenanthrene-9-carboxylate (**9**, 700 mg, 2.15 mmol) was converted into the target compound **16** (730 mg, 1.74 mmol, 81%) which was obtained as a yellow waxy solid.

^{1}H-NMR (400 MHz, $CDCl_3$): δ/ppm 7.71 (s, 1H), 7.65 (s, 1H), 7.63 (d, *J* = 2.5 Hz, 1H), 7.61 (d, *J* = 8.8 Hz, 1H), 7.50 (s, 1H), 7.49 (s, 1H), 7.10 (dd, *J* = 8.7, 2.4 Hz, 1H), 7.06 (t, *J* = 5.9, 5.9 Hz, 1H), 6.99 (t, *J* = 1.1 Hz, 1H), 6.93 (t, *J* = 1.3 Hz, 1H), 4.03 (s, 3H), 4.01 (t, *J* = 6.8 Hz, 2H), 3.97 (s, 3H), 3.92 (s, 3H), 3.43 (app q, *J* = 6.8 Hz, 2H), 2.07 (p, *J* = 6.8 Hz, 2H). **^{13}C-NMR (100 MHz, $CDCl_3$):** δ/ppm 170.5 (C), 159.2 (C), 149.6 (C), 149.1 (C), 137.2 (CH), 131.9 (C), 130.7 (CH), 129.4 (CH), 129.1 (C), 124.8 (C), 124.7 (CH), 124.2 (C), 124.1 (C), 118.9 (CH), 115.9 (CH), 106.4 (CH), 103.7 (CH), 103.2 (CH), 55.9 (CH_3), 55.8, (CH_3), 55.5 (CH_3), 44.8 (CH_2), 37.2 (CH_2), 31.2 (CH_2). **IR (neat, ν/cm^{-1}):** 3259 (broad), 2939 (m), 1618 (m), 1522 (s), 1508 (s), 1473 (s), 1270 (s), 1228 (s), 1206 (s), 1158 (m), 1033 (m), 832 (w), 734 (w). **HR-MS** (TOF AP+) calculated for $C_{24}H_{26}N_3O_4$ 420.1923, found 420.1921. **HP-LC** (220 nm) Rt = 1.64 min (98% purity).

(*E*)-*N*-(3-(1*H*-Imidazol-1-yl)propyl)-2-(3,4-dimethoxyphenyl)-3-(4-methoxyphenyl)prop-2-en-1-amine, **17**: To a solution of (*E*)-*N*-(3-(1*H*-imidazol-1-yl)propyl)-2-(3,4-dimethoxyphenyl)-3-(4-methoxyphenyl)acryl amide (**15**, 500 mg, 1.19 mmol) in dry THF (10 mL, 0.12 M) was added lithium aluminium hydride (LAH, 200 mg, 5.26 mmol) in portions at room temperature. After 2 h the reaction mixture was carefully quenched by addition of ethyl acetate (1 mL) and water (3 mL). The resulting emulsion was filtered through a pad of celite (ca. 10 g) and washed with ethyl acetate (30 mL). The resulting pale-yellow solution was evaporated to dryness yielding a yellow oil that was purified by column chromatography on silica (20–40% EtOAc/hexanes). The desired product **17** was obtained as a colorless oil that solidified upon standing (445 mg, 1.09 mmol, 92%).

^{1}H-NMR (400 MHz, $CDCl_3$): δ/ppm 7.40 (s, 1H), 7.33–7.29 (m, 2H), 7.06–7.03 (m, 2H), 7.02 (s, 1H), 6.92–6.86 (m, 3H), 6.82 (s, 1H), 6.77 (s, 1H), 3.96 (t, *J* = 6.9 Hz, 2H), 3.91 (s, 3H), 3.89 (s, 3H), 3.82 (s, 3H), 3.75 (s, 2H), 2.54 (t, *J* = 6.6 Hz, 2H), 1.82 (p, *J* = 6.8 Hz, 2H). **^{13}C-NMR (100 MHz, $CDCl_3$):** δ/ppm 158.6 (C), 149.0 (C), 148.7 (C), 138.3 (C), 137.2 (CH), 134.5 (C), 130.0 (2CH + C), 129.4 (CH), 129.1 (CH), 118.9 (CH), 118.7 (CH), 113.8 (2CH), 111.2 (CH), 109.9 (CH), 56.0 ($2CH_3$), 55.3 (CH_3), 48.3 (CH_2), 45.8 (CH_2), 44.6 (CH_2), 31.1 (CH_2). **IR (neat, ν/cm^{-1}):** 2935 (w), 2836 (w), 1670 (m), 1604 (m), 1509 (s), 1463 (m), 1246 (s), 1176 (m), 1143 (m), 1024 (s), 812 (m), 765 (m), 731 (s), 683 (m), 531 (m). **HR-MS** (TOF-AP+) calculated for $C_{24}H_{30}N_3O_3$ 408.2287, found 408.2285. **HP-LC** (220 nm) Rt = 1.52 min (96% purity).

3-(1*H*-Imidazol-1-yl)-N-((3,6,7-trimethoxyphenanthren-9-yl)methyl)propan-1-amine, 18: In analogy to the preparation of compound **17**, *N*-(3-(1H-imidazol-1-yl)propyl)-3,6,7-trimethoxyphenanthrene-9-carboxamide (**16**, 500 mg, 1.19 mmol) was converted to the target compound that was isolated as a waxy solid (454 mg, 1.12 mmol, 94%).

^{1}H-NMR (400 MHz, $CDCl_3$): δ/ppm 7.80 (s, 1H), 7.75 (d, *J* = 2.4 Hz, 1H), 7.68 (d, *J* = 8.7 Hz, 1H), 7.40–7.45 (m, 2H), 7.36 (s, 1H), 7.13 (dd, *J* = 8.7, 2.4 Hz, 1H), 6.96 (t, *J* = 1.1 Hz, 1H), 6.78 (t, *J* = 1.1 Hz, 1H), 4.04 (s, 2H), 4.02 (s, 3H), 3.97 (s, 3H), 3.94 (s, 3H), 3.91–3.95 (m, 2H), 2.64 (t, *J* = 6.7 Hz, 2H), 1.87 (app p, *J* = 6.7 Hz, 2H). **^{13}C-NMR (100 MHz, $CDCl_3$):** δ/ppm 158.1 (C), 149.2 (C), 148.7 (C), 137.1 (CH), 130.8 (C), 130.5 (C), 129.9 (CH), 129.3 (CH), 126.2 (C), 125.7 (C), 124.9 (C), 124.6 (CH), 118.9 (CH), 115.5 (CH), 104.8 (CH), 103.8 (CH), 103.7 (CH), 56.0 (CH_3), 55.9 (CH_3), 55.5 (CH_3), 52.5 (CH_2), 46.3 (CH_2), 44.7 (CH_2), 31.5 (CH_2). **IR (neat, ν/cm^{-1}):** 3002 (w), 2935 (w), 2832 (w), 1609 (s), 1523 (s), 1509 (s), 1467 (s), 1269 (s), 1205 (s), 1161 (m), 1070 (m), 1032 (m), 834 (w), 731 (m). **HR-MS** (TOF AP+) calculated for $C_{24}H_{28}N_3O_3$ 406.2131, found 406.2137. **HP-LC** (220 nm) Rt = 1.46 min (95% purity).

3,6,7-Trimethoxy-11,12,13,14,14a,15-hexahydro-9*H*-dibenzo[*f*,*h*]pyrido[1,2-*b*]isoquinolin-15-ol (19a and 19b): To a solution of 3,6,7-trimethoxy-12,13,14,14a-tetrahydro-9*H*-dibenzo[f,h]pyrido [1,2-b]isoquinolin-15(11*H*)-one (**13**, 250 mg, 0.64 mmol) in dry THF (10 mL, 0.06 M) was slowly added lithium aluminium hydride (73 mg, 1.92 mmol, 3.0 equiv.). After stirring at room temperature for 1 h the mixture was carefully quenched by addition of ethyl acetate (1 mL) and water (1 mL). Filtration over a pad of celite (ca. 5 g) and elution with ethyl acetate (20 mL) yielded after evaporation the crude mixture of **19a** and **19b** (213 mg, 0.54 mmol, 85%) in a 1:2 ratio as evidenced by 1H NMR. The separation of this mixture was accomplished by preparative thin layer chromatography (2 runs) using EtOAc/hexanes (30:70) as solvent system.

Rac-(14*aR*,15*S*)-3,6,7-Trimethoxy-11,12,13,14,14*a*,16-hexahydro-9*H*-dibenzo[*f*,*h*]pyrido-[1,2-*b*]isoquinolin-15-ol, 19a:

^{1}H-NMR (700 MHz, $CDCl_3$): δ/ppm 8.30 (d, *J* = 9.1 Hz, 1H), 7.82 (d, *J* = 2.6 Hz, 1H), 7.80 (s, 1H), 7.21 (dd, *J* = 9.1, 2.5 Hz, 1H), 6.69 (s, 1H), 4.99 (d, *J* = 5.6 Hz, 1H), 4.10 (s, 3H), 4.01 (s, 3H), 3.93 (d, *J* = 15.0 Hz, 1H), 3.89 (s, 3H), 3.03 (br s, 1H), 2.44 (br s, 2H), 2.10 (s, 1H), 1.83 (d, *J* = 12.7 Hz, 1H), 1.75 (d, *J* = 14.3 Hz, 1H), 1.64 (d, *J* = 13.8 Hz, 1H), 1.41 (q, *J* = 12.7 Hz, 1H). 3 Resonances were not observed due to broadening effects. **^{13}C-NMR (176 MHz, $CDCl_3$):** δ/ppm 157.7 (C), 149.4 (C), 148.9 (C), 131.1 (C), 127.5 (CH), 124.1 (C), 124.0 (C), 123.8 (C), 114.8 (CH), 104.6 (CH), 103.7 (CH), 103.2 (CH), 70.3 (CH), 65.5 (CH), 55.9 (CH_3), 55.8 (CH_3), 55.5 (CH_3), 54.5 (CH_2), 23.3 (CH_2). 5 Resonances were not observed (2 C, 3 CH_2). **IR (neat, ν/cm^{-1}):** 3300 (broad), 2936 (m), 1732 (w), 1615 (m), 1514 (s), 1471 (s), 1426 (m), 1262 (s), 1235 (m), 1206 (s), 1172 (m), 1147 (m), 1039 (s), 914 (m), 840 (m), 731 (m). **HR-MS** (ESI-TOF+) calculated for $C_{24}H_{28}NO_4$ 394.2018, found 394.2028. **HP-LC** (220 nm) Rt = 1.76 min (95% purity).

Rac-(14*aR*,15*R*)-3,6,7-Trimethoxy-11,12,13,14,14*a*,16-

hexahydro-9*H*-dibenzo[*f*,*h*]pyrido-[1,2-*b*]isoquinolin-15-ol, 19b: **^{1}H-NMR (600 MHz, $CDCl_3$):** δ/ppm 8.35 (d, $J = 9.0$ Hz, 1H), 7.68 (d, $J = 2.6$ Hz, 1H), 7.50 (s, 1H), 7.21 (dd, $J = 9.0$, 2.5 Hz, 1H), 5.91 (s, 1H), 4.59 (d, $J = 2.5$ Hz, 1H), 4.07 (s, 3H), 4.02 (s, 3H), 3.71 (s, 3H), 2.84–3.00 (m, 2H), 2.80 (d, $J = 14.9$ Hz, 1H), 2.24 (qd, $J = 13.3$, 3.8 Hz, 1H), 2.07 (d, $J = 11.2$ Hz, 1H), 1.90–2.00 (m, 2H), 1.82 (q, $J = 13.1$ Hz, 1H), 1.73 (d, $J = 13.1$, Hz, 1H), 1.67 (d, $J = 12.2$ Hz, 1H), 1.27–1.35 (m, 1H). **^{13}C-NMR (151 MHz, $CDCl_3$):** δ/ppm 157.4 (C), 148.5 (C), 148.3 (C), 130.4 (C), 127.8 (C), 126.8 (CH), 124.7 (C), 124.0 (C), 123.5 (2C), 111.4 (CH), 104.0 (CH), 102.9 (CH), 102.5 (CH), 66.5 (CH), 62.5 (CH), 56.7 (CH_2), 55.6 (CH_3), 55.4 (CH_3), 55.3 (CH_3), 55.2 (CH_2), 27.0 (CH_2), 25.1 (CH_2), 24.1 (CH_2). **IR (neat, ν/cm^{-1}):** 3184 (broad), 2938 (m), 1743 (w), 1611 (m), 1534 (m), 1511 (s), 1470 (s), 1424 (m), 1257 (s), 1204 (s), 1171 (s), 1127 (m), 1042 (s), 910 (m), 839 (m), 730 (s). **HR-MS** (ESI-AP+) calculated for $C_{24}H_{28}NO_4$ 394.2018, found 394.1990. **HP-LC** (220 nm) Rt = 1.77 min (96% purity). *Crystal data for **19b***: $C_{25}H_{29}Cl_2NO_4$, M = 478.39, orthorhombic, space group Pbca, a = 12.2463(8), b = 25.3267(16), c = 29.2135(18) Å, U = 9060.8(10) Å^3, F(000) = 4032, Z = 16, $D_c = 1.403$ mg m^{-3}, $\mu = 0.320$ mm^{-1} (Mo-Kα, $\lambda = 0.71073$ Å), T = 120(1)K. Crystallographic data for the structure have been deposited with the Cambridge Crystallographic Data Centre as supplementary publication CCDC-1842540.

3.2. Biological evaluation

3.2.1. Cells culture

Hepatocellular carcinoma cell lines (Huh7, FOCUS, Hep3B, HepG2 and Mahlavu), human breast carcinoma cells (MCF7) and human colon carcinoma cells (HCT116) were grown in Dulbecco's Modified Eagles Medium (DMEM) supplemented with 10% fetal bovine serum (GIBCO, Invitrogen), 1% non-essential amino acids (GIBCO, Invitrogen) and SNU-475 were grown in RPMI-1640 media (Invitrogen GIBCO) supplemented with 10% FBS, 2 mM L-glutamine. All media contained 100 units/ml penicillin and streptomycin and cells were maintained at 37 °C in a humidified incubator under 5% CO_2.

3.2.2. NCI-60 sulforhodamine B assay

Cells were plated in 96-well plates (HCT116 – 3000, Huh7, Hep3B, HepG2, MCF-7 –2000, Mahlavu, FOCUS, SNU475-1000 cells per well) and grown for 24 h in an incubator. The compounds were dissolved in DMSO and were prepared 20 mM stock solution. The compounds were tested starting from 40 μM to 2,5 μM in triplicates. The compounds, which were below 2,5 μM, were tested starting from 2,5 μM to 0,03 μM. After 72 h of incubation, cells were fixed using 10% (v/v) trichloroacetic acid (MERCK) for an hour. The fixed plates were dried and samples were stained with sulforhodamine B (SRB) solution (50 μl of a 0.4% (m/v) of SRB in 1% acetic acid solution) for 10 min. The excess amount of SRB dye was discarded by washing samples with 1% acetic acid and left for air-drying. The protein bound SRB dye was dissolved in 10 mM Tris-base and its absorbance was measured with 96-well plate reader at 515 nm. The IC_{50} values were calculated based on DMSO control normalization.

3.2.3. Real-time cell growth surveillance by electronic sensing (RTCA)

Real-time cell growth analysis was performed using the xCELLigence System (Roche Applied Sciences). The Huh7 (2000) and Mahlavu (1000) cells were plated in 96 well E plates. In proliferation step, the cellular growth was analyzed with cell index measurements in 30 min intervals. After 24 h of incubation, when cells reach the log growth phase, they were treated with Boehmeriasin derivatives compounds starting from 1 μM to 2 folds serial diluted 4 times. The cell index values (CI) were initially monitored every 10 min for 24 h and then CI were recorded in 30 min intervals. After 72 h of incubation, the cellular growth inhibition was calculated based on the DMSO normalization.

3.2.4. DCHF-DA staining for ROS detection

Huh7 cells were plated into 6 well plates and treated with 1 μM Boehmeriasin derivatives. After treatment, samples were washed with PBS 3 times, they were incubated with DCFH-DA assay solution for 15 min in humidified chamber at 37 °C. The solution was aspirated, and cells were washed with PBS 2 times. The staining was analyzed with fluorescence microscope.

3.2.5. Western blot analysis

Huh7 and Mahlavu cells were treated with the Boehmeriasin derivatives compounds (IC_{100} concentrations) or with DMSO control for 48 h. After incubation period, the cells were collected with scraper, their total proteins were isolated and protein concentrations were calculated with Bradford assay. 20–50 μg from all proteins were loaded to Bis-Tris gel and western blot was performed with Novex® NuPAGE® Bis-Tris Electrophoresis system. Then the proteins were transferred to nitrocellulose membrane via XCell IITM Blot Module. Cyclin-B1 (554,177, BD), Cdc2/Cdk1 (PC25, Calbiochem), PARP (9532, Cell Signaling), Cyclin E (CC05, Calbiochem), Cdk2 (sc6248, Santa Cruz), phosphor ASK1 (3765, Cell Signaling), phosphor SAPK/JNK (9251, Cell Signaling), phosphor AKT (9275, Cell Signaling) and AKT (9272, Cell Signaling) antibodies were used in 1:100 to 1:500 5% BSA-TBS-T. β-actin (#A5441, Sigma) and Calnexin (C4731, Sigma) antibodies were used in 1:1000 concentration for equal loading.

3.2.6. Immunofluorescence assay

Huh7 and Mahlavu cells were seeded in 6 well plates on coverslips. After 24 h, cells were treated with the 1 μM Boehmeriasin derivatives for 72 h. Camptothecin was used as positive control for cytochrome c activity. DMSO control were given to cells in the same amount of the compounds. After the incubation period, cells were fixed with ice-cold methanol for 15 min. The cytochrome c primary antibody (Santa Cruz, 1:100 in 0,1% TBS-Tween) were applied for 1 h. FITC conjugated secondary antibody (Santa Cruz, 1:200 in 0,1% TBS-Tween) were applied for 1 h. The cells were mounted with UltraCruz DAPI mounting medium and photos were taken with fluorescence microscopy.

3.2.7. Flow cytometry for cell cycle analysis

Huh7 and Mahlavu cells were seeded onto 100 mm culture dishes. After 24 h, cells were treated with the 1 μM Boehmeriasin derivatives. After 24 h, 48 h and 72 h of incubation, cells were fixed with ice-cold 70% ethanol for 3 h at −20 °C. Cell cycle analysis was carried out by PI (Propidium Iodide) staining using MUSE Cell Analyzer according to the manufacturer's recommendations (Millipore).

3.2.8. Flow cytometry for annexin

30.000 Mahlavu and 60.000 Huh7 cells were plated to 6 wells. After 24 h, cells were treated with 1 μM of **1**, **19**, **19a** and **19b**. The cells were collected with trypsin after 24, 48 and 72 h of treatment. The supernatants were also collected into same tube. The cells were centrifuged at 1600 rpm for 6 min and 100 μL of annexin stain solution was added on top of the pellets. The cells were incubated for 15 min with stain solution in the dark. Before analyzing the samples, 400 μL 1xPBS was added and cells were resuspended. The Annexin V samples were analyzed with a Novocyte Flow Instrument.

Annexin stain solution (Roche-11988549001):

2 μl Annexin-V-FLUOS labeling reagent and 2 μL propidium iodide solution were added in 100 μl Incubation buffer per sample.

3.2.9. Hoechst nuclear staining

30.000 Mahlavu and 60.000 Huh7 cells were plated to 6 wells on to coverslips. After 24 h, cells were treated with 1 μM of **1**, **19**, **19a** and **19b**. The cells were fixed with ice-cold ethanol after 24 and 72 h of treatment. Samples were washed with 1X PBS three times and samples were incubated via Hoechst staining solution for 10 min. Samples were washed with distilled water and mounted with glycerol. Hoechst staining was analyzed via fluorescence microscopy (Nikon).

Author contributions

The manuscript was written through contributions of all authors. All authors have given approval to the final version of the manuscript.

Acknowledgment

We gratefully acknowledge funding from the Royal Society (to MB and IRB), the British Council for a travel grant (to MB) and Turkish Ministry of Development Kansil_2016K121540 project (to RA and EA). The School of Chemistry at University College Dublin is acknowledged for providing start-up support (to MB). Finally, we are thankful to Dr Andrei Batsanov (University of Durham) for solving the X-ray structure of compound **19b**.

Appendix A. Supplementary data

Supplementary data to this article can be found online at https://doi.org/10.1016/j.ejmech.2019.01.056.

Abbreviations

CCR2	CC chemokine receptor 2
CCL2	CC chemokine ligand 2
CCR5	CC chemokine receptor 5
PARP	Poly (ADP-ribose) polymerase
CDI	carbonyl diimidazole
TLC	thin layer chromatography
LAH	lithium aluminum hydride

References

[1] J. Ferlay, I. Soerjomataram, R. Dikshit, S. Eser, C. Mathers, M. Rebelo, D.M. Parkin, D. Forman, F. Bray, Cancer incidence and mortality worldwide: sources, methods and major patterns in GLOBOCAN 2012, Int. J. Canc. 136 (2015) E359–E386.
[2] H.B. El-Serag, Hepatocellular carcinoma, N. Engl. J. Med. 365 (2011) 1118–1127.
[3] F.X. Bosch, J. Ribes, R. Cleries, M. Diaz, Epidemiology of hepatocellular carcinoma, Clin. Liver Dis. 9 (2005) 191–211.
[4] H.B. El-Serag, K.L. Rudolph, Hepatocellular carcinoma: epidemiology and molecular carcinogenesis, Gastroenterology 132 (2007) 2557–2576.
[5] Z.A. Sherif, A. Saeed, S. Ghavimi, S.M. Nouraie, A.O. Laiyemo, H. Brim, H. Ashktorab, Global epidemiology of non-alcoholic fatty liver disease and perspectives on US minority populations, Dig. Dis. Sci. 61 (2016) 1214–1225.
[6] P.A. Farazi, R.A. DePinho, Hepatocellular carcinoma pathogenesis: from genes to environment, Nat. Rev. Canc. 6 (2006) 674–687.
[7] M. Hertl, A.B. Cosimi, Liver transplantation for malignancy, Oncol. 10 (2005) 269–281.
[8] J.M. Llovet, S. Ricci, V. Mazzaferro, P. Hilgard, E. Gane, J.F. Blanc, A.C. de Oliveira, A. Santoro, J.L. Raoul, A. Forner, M. Schwartz, C. Porta, S. Zeuzem, L. Bolondi, T.F. Greten, P.R. Galle, J.F. Seitz, I. Borbath, D. Häussinger, T. Giannaris, M. Shan, M. Moscovici, D. Voliotis, J. Bruix, Sorafenib in advanced hepatocellular carcinoma, N. Engl. J. Med. 359 (2008) 378–390.
[9] J. Brui, S. Qin, P. Merle, A. Granito, Y.-H. Huang, G. Bodoky, M. Pracht, O. Yokosuka, O. Rosmorduc, V. Breder, R. Gerolami, G. Masi, P.J. Ross, T. Song, J.-P. Bronowicki, I. Ollivier-Hourmand, M. Kudo, A.-L. Cheng, J.M. Llovet, R.S. Finn, M.-A. LeBerre, A. Baumhauer, G. Meinhardt, G. Han, Regorafenib for patients with hepatocellular carcinoma who progressed on sorafenib treatment (RESORCE): a randomised, double-blind, placebo-controlled, phase 3 trial, Lancet 389 (2017) 56–66.
[10] S. Richard, P. Finn, A. Merle, A. Granito, B. Jordi, Outcomes with sorafenib (SOR) followed by regorafenib (REG) or placebo (PBO) for hepatocellular carcinoma (HCC): results of the international, randomized phase 3 RESORCE trial, J. Clin. Oncol. 35 (4_suppl) (2017) 344.
[11] Y. Luo, Y. Liu, D. Luo, X. Gao, B. Li, G. Zhang, Cytotoxic alkaloids from Boehmeria siamensis, Planta Med. 69 (2003) 842–845.
[12] M. Cui, Q. Wang, Total synthesis of phenanthrol-quinolizidine alkaloids: (±)-cryptopleurine, (±)-boehmeriasin A, (±)-boehmeriasin B and (±)-hydroxycryptopleurine, Eur. J. Org. Chem. 31 (2009) 5445–5451.
[13] H. Wei, J. Yan, J. Liu, D. Luo, G. Zhang, Induction of G1 arrest and differentiation in MDA-MB-231 breast cancer cells by boehmeriasin A, a novel compound from plant, Int. J. Gynecol. Canc. 16 (2006) 165–170.
[14] S.R. Chemler, Phenanthroindolizidines and phenanthroquinolizidines: promising alkaloids for anti-cancer therapy, Curr. Bioact. Compd. 5 (2009) 2–19.
[15] S. Saraswati, P.K. Kanaujia, S. Kumar, R. Kumar, A.A. Alhaider, Tylophorine, a phenanthraindolizidine alkaloid isolated from *Tylophora indica* exerts anti-angiogenic and antitumor activity by targeting vascular endothelial growth factor receptor 2-mediated angiogenesis, Mol. Canc. 12 (2013) 82.
[16] C.-W. Yang, Y.-Z. Lee, H.-Y. Hsu, C.-M. Wu, H.-Y. Chang, Y.-S. Chao, S.-J. Lee, c-Jun-mediated anticancer mechanisms of tylophorine, Carcinogenesis 34 (2013) 1304–1314.
[17] E.-H. Kim, H.-Y. Min, H.-J. Chung, J. Song, H.-J. Park, S. Kim, S.K. Lee, Antiproliferative activity and suppression of P-glycoprotein by (−)-antofine, a natural phenanthroindolizidine alkaloid, in paclitaxel-resistant human lung cancer cells, Food Chem. Toxicol. 50 (2012) 1060–1065.
[18] Y. Fu, S.K. Lee, H.-Y. Min, T. Lee, J. Lee, M. Cheng, S. Kim, Synthesis and structure-activity studies of antofine analogues as potential anticancer agents, Bioorg. Med. Chem. Lett 17 (2007) 97–100.
[19] Y. Kwon, J. Song, H. Lee, E.-Y. Kim, K. Lee, S.K. Lee, S. Kim, Design, synthesis, and biological activity of sulfonamide analogues of antofine and cryptopleurine as potent and orally active antitumor agents, J. Med. Chem. 58 (2015) 7749–7762.
[20] Antofine and Cryptopleurine Derivatives as Anticancer Agents. US Patent US20120283220A1 (published Nov 8, 2012).
[21] H.R. Jin, S.Z. Jin, X.F. Cai, D. Li, X. Wu, J.X. Nan, J.J. Lee, X. Jin, Cryptopleurine targets NF-κB-Pathway, leading to inhibition of gene products associated with cell survival, proliferation, invasion, and angiogenesis, PLoS One 7 (2012), e40355.
[22] W. Zing, J.W. Herndon, Total synthesis of (+)-Antofine and (−)-Cryptopleurine, Eur. J. Org. Chem. (2013) 3112–3122.
[23] A. Fürstner, J.W.J. Kennedy, Total syntheses of the Tylophora alkaloids cryptopleurine, (−)-Antofine, (−)-Tylophorine, and (−)-Ficuseptine C, Chem. Eur J. 12 (2006) 7398–7410.
[24] M.S. Christodoulou, F. Calogero, M. Baumann, A.N. Garcia-Argaez, S. Pieraccini, M. Sironi, F. Dapiaggi, R. Bucci, G. Broggini, S. Gazzola, S. Liekens, A. Silvani, M. Lahtela-Kakkonen, N. Martinet, A. Nonell-Canals, E. Santamaria-Navarro, I.R. Baxendale, L. Dalla Via, D. Passarella, Boehmeriasin A as new lead compound for the inhibition of topoisomerases and SIRT2, Eur. J. Med. Chem. 92 (2015) 766–775.
[25] I. Durmaz, E.B. Guven, T. Ersahin, M. Ozturk, I. Calis, R. Cetin-Atalay, Liver cancer cells are sensitive to Lanatoside C induced cell death independent of their PTEN status, Phytomedicine 23 (2016) 42–51.
[26] M.B. Iecermak, G. Ince, M. Ozturk, R. Cetin-Atalay, Acquired tolerance of hepatocellular carcinoma cells to selenium deficiency: a selective survival mechanism? Cancer Res. 63 (2003) 6707–6715.